Date: May 1, 2025

Cancer Immune Monitoring and Analysis Center
Dana-Farber Cancer Institute
Harvard Medical School
Contact PI: Catherine J. Wu, MD (e-mail: Catherine_wu@dfci.harvard.edu)

Performance lab:
Translational Immunogenomics Lab (TIGL)
Catherine J. Wu, MD (Faculty Advisor)
Kenneth J. Livak, PhD (Technology Lead Scientist)
Shuqiang Li, PhD (Technology Lead Scientist)

Scientific lab:
Erin Parry (Principal Investigator)

Visium Spatial RNA Profiling Analytical Performance Report, version 1

1. Intended Use

Single cell RNA sequencing (scRNAseq) has become the definitive method for determining cell types and cell states,[1] but the method relies on dispersed single cells and thus information about cellular organization in tissues and cell-to-cell relationships is lost. The advent of spatial transcriptomics addresses this deficiency because these technologies enable transcriptome-wide quantification of RNAs in intact tissue sections (reviewed by Tian *et al.*[2]). These methods are used to determine the cell-type composition and architecture of tissues, to characterize cell-cell interactions, and to investigate molecular interactions such as receptor-ligand pairs. We have focused our analysis on formalin-fixed paraffin embedded (FFPE) samples because these are routinely collected as part of clinical diagnostics and because it enables the analysis of archived biobank samples, including those collected on clinical trials. The probe-based Visium system from 10x Genomics is well-suited to the study of FFPE samples because of its tolerance for the degraded RNA caused by the fixation and embedding process. As shown in **Figure 1A**, the initial incarnation of Visium used a low-resolution spatial barcode array for the analysis of multi-cell patches. The denser Visium HD array shown in **Figure 1B** enables obtaining results that approach single-cell resolution. We are reporting results for both Visium and Visium HD.

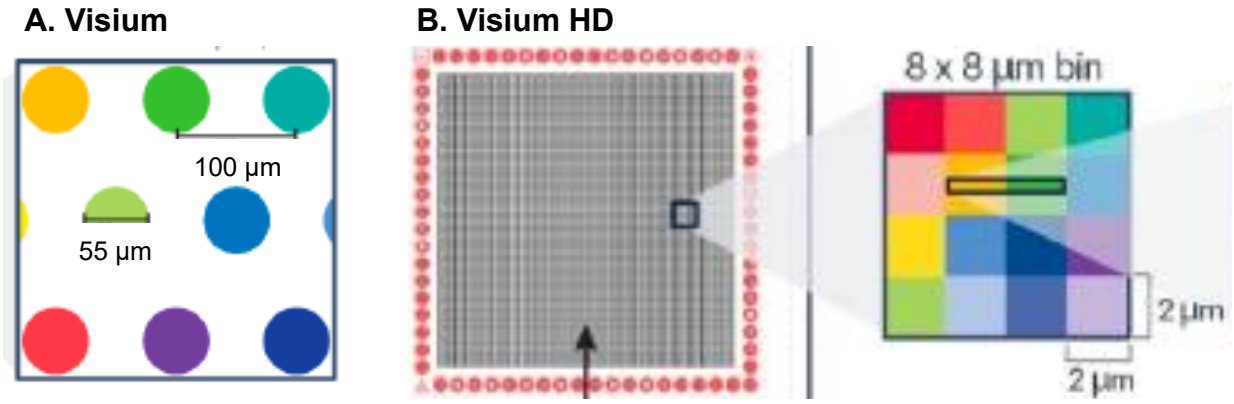

Figure 1. Comparison of oligonucleotide barcode arrays for Visium and Visium HD. **A. Visium**. 6.5×6.5 mm capture area with 5,000 55-µm barcoded spots at 100 µm center-to-center spacing. **B. Visium HD**. 6.5×6.5 mm capture area with continuous lawn of 11,000,000 2-µm barcoded squares. For analysis, results from 2-µm squares are aggregated into 8×8 µm bins, which is roughly the size of a single cell.

The following two trials assigned to DFCI have Visium listed and approved in the biomarker table:

- A151804 (Dr Kozono, PACT)

- EA6194 (Dr Tahini, CIMAC)

There are three additional trials with Visium currently assigned to Mt Sinai, for which DFCI could serve as a backup:

- CA027-005
- GU16-257
- 10104

Table 1. Summary of analytical performance findings for Visium Spatial RNA Profiling

Accuracy	Accuracy was qualitatively assessed by comparing to the spatial distribution of cell types in distinct morphological features determined by single-cell proteomic detection (**Figure 8**). Accuracy was also assessed by comparison to a scRNAseq dataset from the same tissue type (**Figures 6** and **7**).
Precision	Precision was assessed by comparison of pseudo-bulk RNA expression results from consecutive sections (**Figure 4**). As consecutive sections are not identical in content or placement on the Visium spatial array, this is only an approximation of precision.
Analytical sensitivity	The number of UMI (unique molecular identifier) counts is a measure of transcript quantity. Sensitivity is reported as the number of UMI counts per spot (Visium) or per 8 µm bin (Visium HD). More UMI counts translate to more genes detected per spot or 8 µm bin. For any particular transcript, the detection limit is 1 UMI per spot or 8 µm bin.
Analytical specificity including interfering substances	Specificity is determined by the probe design of 10x Genomics. Although genomic DNA would be an interfering substance, its contribution to experimental signal is essentially eliminated by rigorous mapping to the transcript-specific probe set (see “Reads confidently mapped to probe set” in **Tables 3** and **4**).
Reportable range	3 - 24,210 UMI counts per spot and 3 - 7,943 genes per spot for Visium. 3 – 1,396 UMI counts per spot and 2 – 1,046 genes per 8 µm bin for Visium HD.
Reference interval (normal range)	Not applicable.
Standardization, harmonization, reproducibility, and ruggedness	Standardization and ruggedness have been achieved by using commercial instrumentation and kits following the manufacturer’s protocol.
Quality control and improvement procedures	Observation of the expected size distribution for the amplified probe library (**Figure 3**) is a prerequisite for proceeding with sequencing. The parameters reported in **Table 3** and **Table 4** are compared to the expected values provided by 10x Genomics to determine if each dataset is suitable for further analysis.
Any other performance data	None

2. Materials and Methods

Biological Specimens

FFPE excisional lymph node biopsy specimens stored in DF/HCC pathology archives were utilized for this study. Prior to analysis, tissue sections were reviewed by an expert hematopathologist to confirm tissue integrity and select representative field of interest for Visium spatial RNA profiling.

We report the data from a pilot of two adjacent sections of two follicular lymphoma excisional lymph node biopsies using the Visium assay (n=4 tissue sections).

Initial results were followed up by Visium HD analysis of 2 additional expert reviewed follicular lymphoma (FL) cases with regions of both indolent (or typical) lymphoma and aggressive (or transformed) lymphoma. Visium HD results were validated by single-cell protein detection.

Additional reference cohorts for comparison included previously generated single-cell transcriptomic data from dissociated typical and transformed FL biopsies (n=10, one of which overlapped with a Visium HD case).[3]

RNA Extraction

A 10-micron scroll was cut from each FFPE block for DV200 analysis. RNA from the scrolls was extracted using the RNeasy FFPE Kit (Qiagen 73504) per manufacturer instructions, and RNA quality and quantity were assessed using the RNA 6000 Pico Kit (Agilent 5067-1513) for the 2100 Bioanalyzer System.

Sectioning

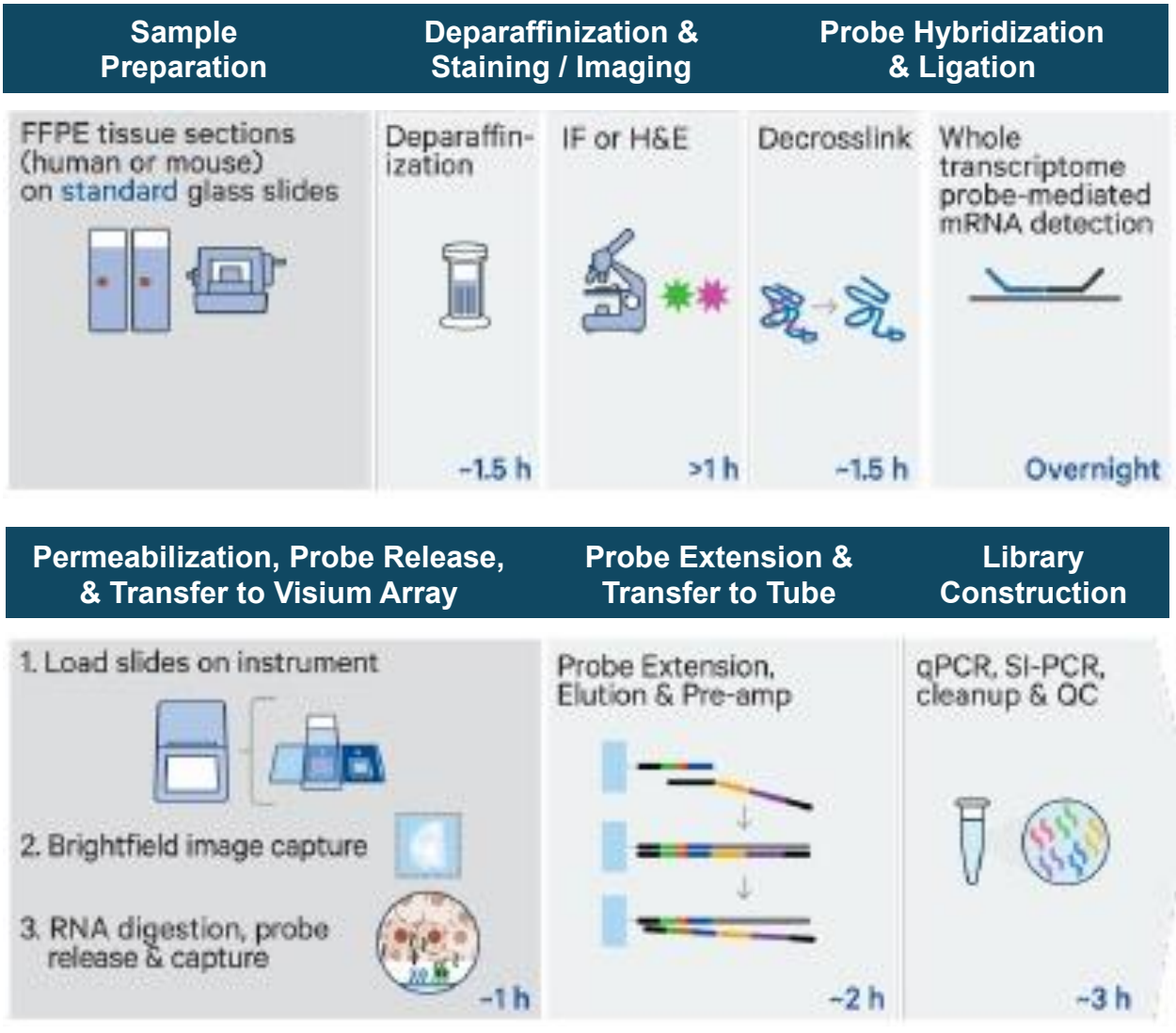

Figure 2. Visium and Visium HD CytAssist spatial gene expression for FFPE workflow.

The steps from tissue sectioning through sequencing library construction are shown in **Figure 2**. Tissue was sectioned at a thickness of 5 microns from FFPE blocks onto Fisherbrand Superfrost Plus Microscope Slides (Cat 12-550-15) in the DF/HCC BWH Pathology Core using RNase-free processing, as outlined in the Visium user manual (CG000518). The DF/HCC BWH Pathology Core has expertise in tissue sectioning

for spatial transcriptomics and proteomics with a dedicated workflow to ensure high-quality initial processing. For the Visium pilot study, tissue sections were deparaffinized and hematoxalin and eosin (H&E) stained in the Parry Laboratory at Dana-Farber following manufacturer's instructions (CG000520). H&E imaging was performed using the THUNDER Imager microscope in the DFCI Molecular Imaging Core. For Visium HD, tissue sectioning was performed using the same methodology as above. Tissue deparaffinization and H&E staining was done according to the Visium HD manual (CG000684) using the staining solutions recommended by 10x Genomics. Whole Visium HD sections were imaged using a Grundium Ocus 40 scanner in the DFCI Pathology Core Lab.

Visium Library Preparation and Sequencing

10x Genomics Visium slides, cassettes, transcriptome probes, and reagents were from the Visium CytAssist for FFPE Spatial Gene Expression 6.5mm Human Kit (1000443) for the Visium pilot study and the Visium HD, Human Transcriptome, 6.5 mm Kit (1000673) for the Visium HD follow-up study. The detailed protocols for the following steps are in User Guide CG000495 for Visium and in User Guide CG000685 for Visium HD. After assembling two slides with the deparaffinized and stained tissue sections into a Tissue Slide Cassette, sections were de-stained and de-crosslinked, the human whole transcriptome probe panel was added to slides, and probe pair hybridization to their complementary target RNA proceeded overnight. Following washing, hybridized probe pairs were ligated. Following placement of the tissue slides and Visium slide in the Visium CytAssist instrument, probe release and probe capture on Visium slide were performed. The Visium slide was assembled into a Visium Cassette to perform probe extension. Eluted barcoded ligation products were transferred to PCR tubes for subsequent amplification, bead clean-up, and sequencing library preparation. The sequencing libraries were quantified using the Bioanalyzer DNA High Sensitivity Kit (Agilent 5067-4626). The libraries were sequenced on the Illumina NextSeq 1000 using P2-100cycle kits (20046811). The sequencing parameters for Visium libraries were: Read 1: 28nt, Read 2: 50nt, Index 1: 10nt, Index 2: 10nt. The sequencing parameters for Visium HD libraries were: Read 1: 43nt, Read 2: 50nt, Index 1: 10nt, Index 2: 10nt.

Data Processing

Raw sequencing reads from Visium and Visium HD assays were demultiplexed and processed using the Visium SpaceRanger 3.0.0 (10x Genomics) and human transcriptome build GRCh38-2020-A. Manual tissue alignment was used given the large sections being analyzed.

3. Results

QC for the Extracted RNA

Table 2. Metrics for RNA extracted from FFPE scrolls determined by Bioanalyzer

	Sample ID	DV200	Concentration (ng/µL)
Visium	FL-DF-65	<30%	23.8
	FL-DF-222	>70%	8.0
Visium HD	FL-33	30-50%	36.0
	FL-14	<30%	18.7

DV200 is the percentage of total RNA fragments >200 nucleotides. 10x Genomics recommends that tissue used with Visium or Visium HD should have a DV200 of >30%. As the results below show, we obtained good results even with samples that had DV200 <30%. This suggests that assessment of DV200 is not a critical parameter in selecting FFPE samples for Visium or Visium HD analysis.

QC for Visium and Visium HD Sequencing Libraries

The Bioanalyzer trace (**Figure 3**) shows that all the sequencing libraries have the sizes expected for amplification of the Visium (240 bp) and Visium HD (250 bp) probes.

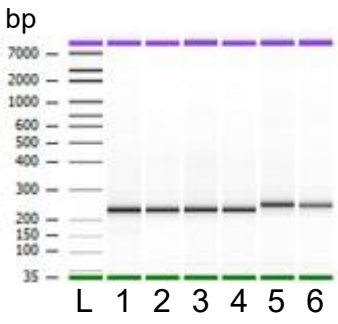

Figure 3. Quality control of Visium and Visium HD sequencing libraries. Agilent Bioanalyzer traces showing the fragment size distribution for each of the samples. L: size ladder. 1: FL-DF-222-S1. 2: FL-DF-222-S2. 3: FL-DF-65-S1. 4: FL-DF-65-S2. 5. FL-33. 6: FL-14.

Space Ranger Metrics

Table 3. Recovery statistics for Visium samples					
Visium sequencing parameter	FL-DF-65-S1	FL-DF-65-S2	FL-DF-222-S1	FL-DF-222-S2	Expected value
Number of reads	70,291,375	71,426,902	182,484,849	146,394,050	Dependent on size of tissue section, placement of section on Visium spatial array, and sequencing depth
Number of spots under tissue	1,525	2,040	4,857	4,677	Same as Number of reads
Mean reads per spot	46,093	35,013	37,572	31,301	>25,000
Median UMI counts per spot	2,153	1,746	1,995	6,702	Dependent on tissue type, RNA quality, and sequencing depth
Range of UMI counts per spot	5 - 13,183	3 -7,603	5 - 12,577	7 -24,210	
Genes detected	18,019	18,028	18,024	18,039	Same as median UMI counts per spot
Median genes per spot	1,699	1,396	1,528	3,980	Same as median UMI counts per spot
Range of genes per spot	5 - 5,984	3 - 4,345	5 - 5,741	7 - 7,943	
Reads confidently mapped to probe set	97.6%	93.1%	86.8%	97.6%	>50%
Valid barcodes	98.9%	98.4%	94.4%	98.9%	>75%
Valid UMIs	100%	100%	100%	100%	>75%
Fraction of reads in spots under tissue	89.8%	90.2%	99.3%	99.7%	>50%
Sequencing saturation	93.6%	93.6%	93.6%	75.7%	Dependent upon sequencing depth and sample complexity but should be >50%

For the pilot Visium analysis, we saw consistent metrics across runs, with reads and genes correlating to areas of tissue in the captured region of interest contained in the set. The higher number of reads and spots seen for the larger of the two tissue sections (FL-DF-222) compared to the smaller section (FL-DF-65) was expected. Reads confidently mapped to probe sets were >85% across all runs, valid barcodes were >95%, and valid UMIs were at 100%. Sequencing saturation was >75%.

Table 4. Recovery statistics for Visium HD samples			
Visium HD sequencing parameter	FL-33	FL-14	Expected value
Number of reads	472,221,805	454,675,706	Dependent on size of tissue section, placement of section on Visium HD spatial array, and sequencing depth

Number of 8 µm binned squares under tissue	701,837	582,846	Same as Number of reads
Mean reads per 8 µm bin	672.8	780.1	Dependent upon sequencing depth and sample complexity
Mean UMIs per 8 µm bin	167.6	222.7	Dependent on tissue type, RNA quality, and sequencing depth
Range of UMIs per 8 µm bin	3 - 1071	3 - 1396	
Genes detected	18,071	18,056	Same as mean UMI counts per spot
Mean genes per 8 µm bin	156.7	201.3	Same as mean UMI counts per spot
Range of genes per 8 µm bin	2 - 898	2 - 1046	
Reads confidently mapped to probe set	97.4%	97.2%	>50%
Valid barcodes	89.0%	89.5%	>75%
Valid UMIs	99.7%	99.7%	>75%
Fraction of 8 µm bins under tissue	99.9%	83.0%	>50%
Sequencing saturation	70.7%	66.3%	Dependent upon sequencing depth and sample complexity but should be >50%

For the Visium HD analysis, we similarly achieved excellent results, with sequencing saturation of 70.7 and 66.3% with sequence depth of 472M and 455M reads. Reads confidently mapped to probe sets were >97%, valid barcodes were approximately 89%, and valid UMIs were >99%.

Visium Analysis

Comparison of consecutive sections. Sections were compared by pseudo-bulk analysis to show reproducibility of the assay. First, adjacent sections derived from the same case displayed high overlap in pseudo-bulk analysis in comparison of gene expression across all Visium runs (Pearson correlation >0.95, **Figure 4A**), reflecting ability to capture case-specific features in sequential runs. Across consecutive sections, transcripts showed high correlation (**Figure 4B-C**).

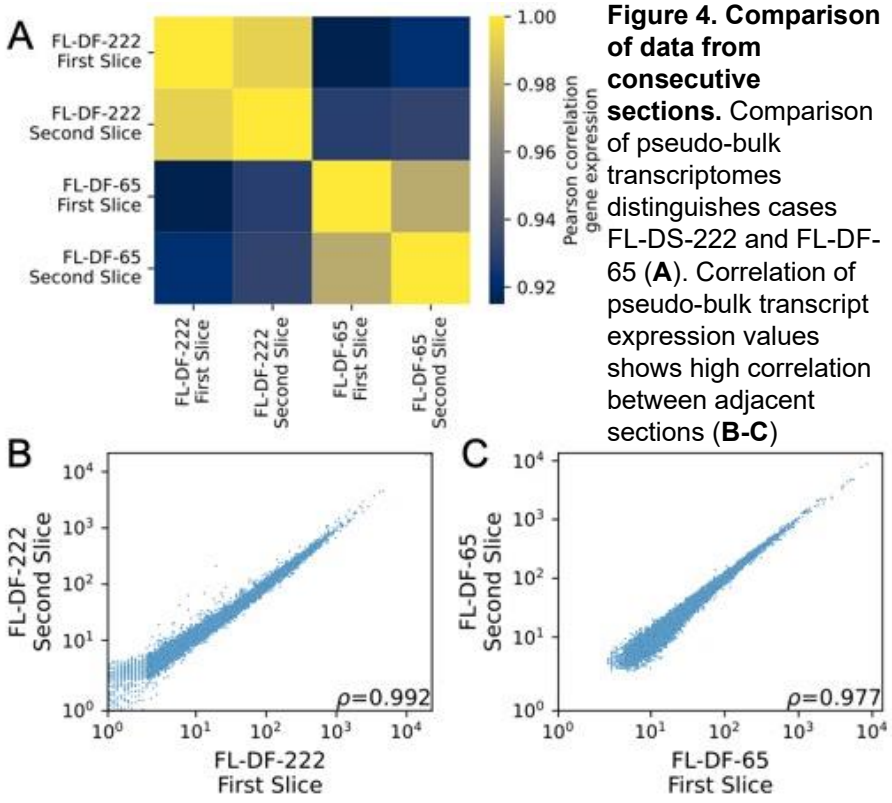

Figure 4. Comparison of data from consecutive sections. Comparison of pseudo-bulk transcriptomes distinguishes cases FL-DS-222 and FL-DF-65 (**A**). Correlation of pseudo-bulk transcript expression values shows high correlation between adjacent sections (**B-C**)

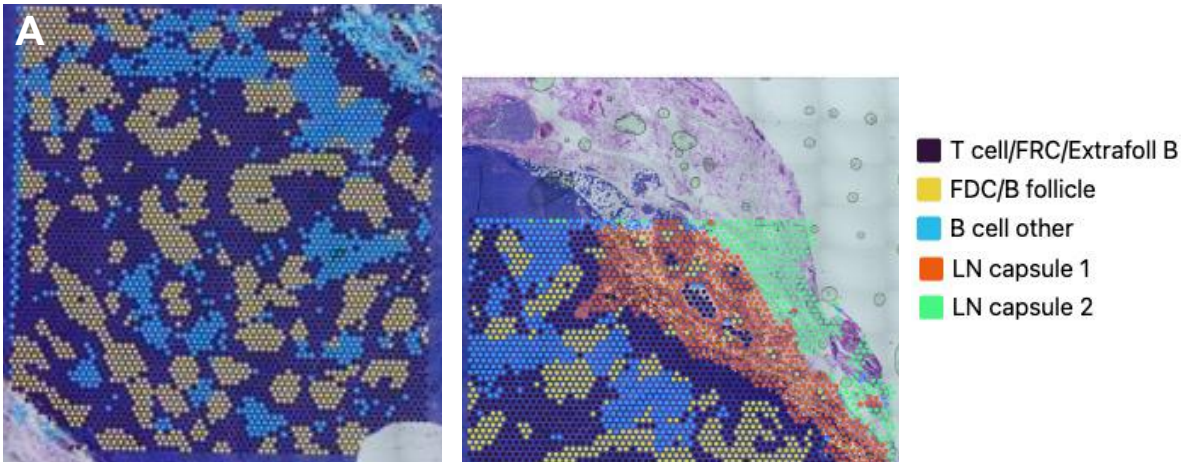

Figure 5. Leiden clustering of adjacent tissue sections. Leiden clustering of transcriptomic data from FL-222-S1 (**A**) and FL-222-S2 (**B**) on tissue sections. FRC - fibroblastic reticular cell; Extrafoll B – extrafollicular B cell; FDC – follicular dendritic cell; LN – lymph node

Identification of cell neighborhoods. FL by definition replaces the normal lymph node architecture with neoplastic follicles of varying cell sizes yet often retains many spatially distinct anatomical structures of normal lymph nodes, including the T-cell zone.[4,5] Recent literature has increasingly identified core features of the microenvironment and stromal populations that are altered in FL.[6–8] Furthermore, the microenvironment is known to have an important role in supporting survival of malignant cell types. Therefore, FL is an ideal setting of a disrupted lymph node microenvironment to deploy spatial profiling. **Figure 5** shows Leiden clustering[9] applied to Visium tissue results to define cell neighborhoods. In FL-DF-222-S1, three major neighborhoods were detected. In FL-DF-222-S2, two additional neighborhoods were identified because a slight shift in tissue orientation enabled capture of lymph node capsular cell types.

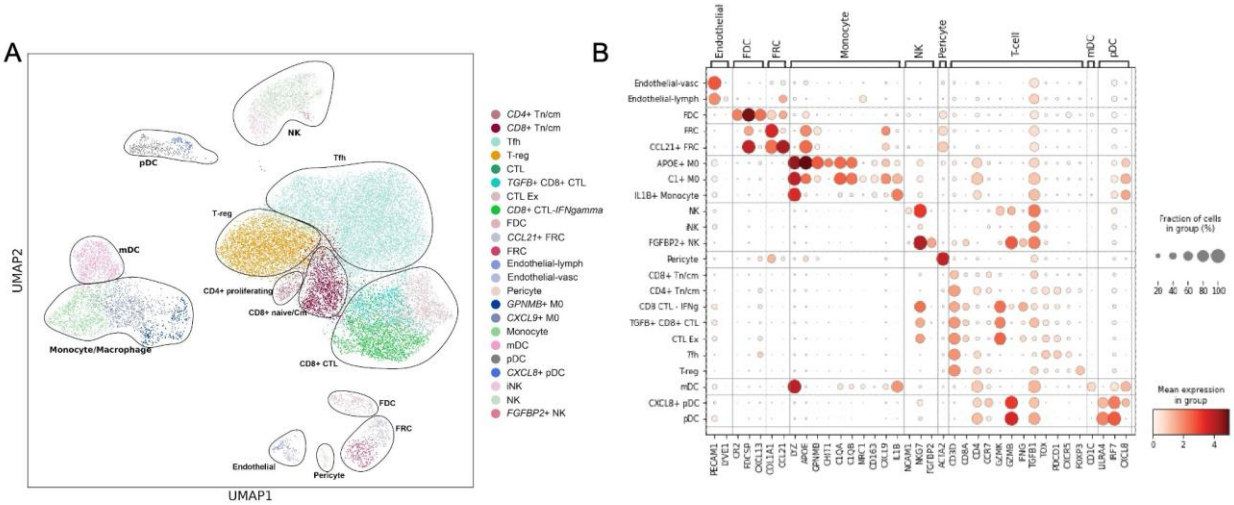

Figure 6. scRNAseq reference. UMAP of identified cell types (key, right) with major cell lineages shown in circles (**A**). Dot plot (**B**) showing marker genes (bottom) for each cell type (left), representing 9 major cell lineages (top). Marker genes: *PECAM1*, *LYVE1*, *CR2*, *FDCSP*, *CXCL13*, *COL1A1*, *CCL21*, *LYZ*, *APOE*, *GPNMB*, *CHIT1*, *C1QA*, *C1QB*, *MRC1*, *CD163*, *CXCL9*, *IL1B*, *NCAM1*, NKG7, *FGFBP2*, *ACTA2*, *CD3D*, *CD8A*, *CD4*, *CCR7*, *GZMK*, *FNG*, *TGFB1*, *TOX*, *PDCD1*, *CXCR5*, *FOXP3*, *CD1C*, *LILRA4*, *IRF7*, *CXCL8*

Comparison to FL cell types. We had previously annotated cell types within the FL lymph node tumor microenvironment by scRNAseq of six FL biopsies and four biopsies in which FL had transformed to aggressive lymphoma (tFL), identifying >47,300 malignant and approximately 24,000 non-malignant cells.[3] Clustering of non-malignant cell types identified nine major cell lineages with sub-clustering revealing additional immune and stromal cell diversity (**Figure 6**). (Included in this single-cell reference was FL-33,

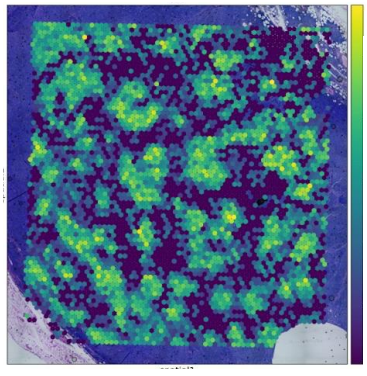

Figure 7. Marker gene in Visium data. RNA expression level of follicular dendritic cell marker gene *CLU* in tissue map for FL-222-S1 from **Figure 5A**.

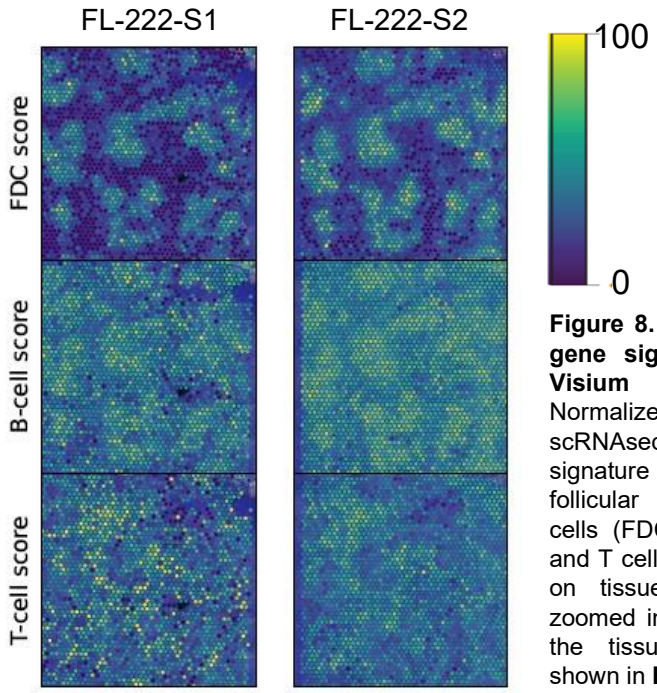

Figure 8. scRNAseq gene signatures in Visium data. Normalized scRNAseq gene signature scores for follicular dendritic cells (FDC), B cells, and T cells projected on tissue map for zoomed in regions of the tissue sections shown in **Figure 5**.

one of the two Visium HD cases.) An indication of Visium sensitivity is that transcripts from all the marker genes listed in **Figure 6B** were detected in Visium results and were localized to the appropriate neighborhoods. As an example, **Figure 7** shows detection of the follicular dendritic cell (FDC) marker *CLU* in FDC/B follicle neighborhoods. Utilization of gene scores from transcriptional populations identified by scRNAseq (e.g., B cell tumor signature) as well as lineage-specific marker genes confirmed cell-neighborhood identities assigned by marker genes. All expected major cellular populations were mapped to spatial data, although the limited resolution of Visium precluded clear identification of interspersed small vessels, endothelium and pericytes. **Figure 8** shows that the localization of gene signature scores are reproducible across adjacent sections.

Visium HD Analysis

Validation of cell type populations by comparison to CODEX proteomic results. We next performed Visium HD analysis of two cases in which we captured FL adjacent to regions of FL transformation to diffuse large B cell lymphoma (DLBCL) histology, or tFL. Thus, we captured two lymphoma microenvironments in a single captured Visium section. In these cases, an expert hematopathologist reviewed and annotated the assigned histology on matching H&E-stained section. Consistent with our prior single-cell and bulk transcriptional data,[3] we found disruption of the follicular structure on transformation with expanded fibroblastic and macrophage/monocyte populations and reduced CD4+ T cells (**Figure 8A**). Major populations were validated with single-cell proteomic analysis by CODEX[10] using a 41-marker protein panel (**Figure 8B**). Further evidence of the concordance of Visium HD and CODEX results is that all the transcripts encoding the CODEX set of proteins were detected by Visium HD in the appropriate neighborhoods. The improved resolution of Visium HD allowed improved capture of defined neighborhoods and structures and allowed us to identify cytokine-signaling interactions and colocalization of macrophages, fibroblasts and pericytes in transformed FL (**Figure 8C**-correlation plot, **Figure 8D**-colocalization).

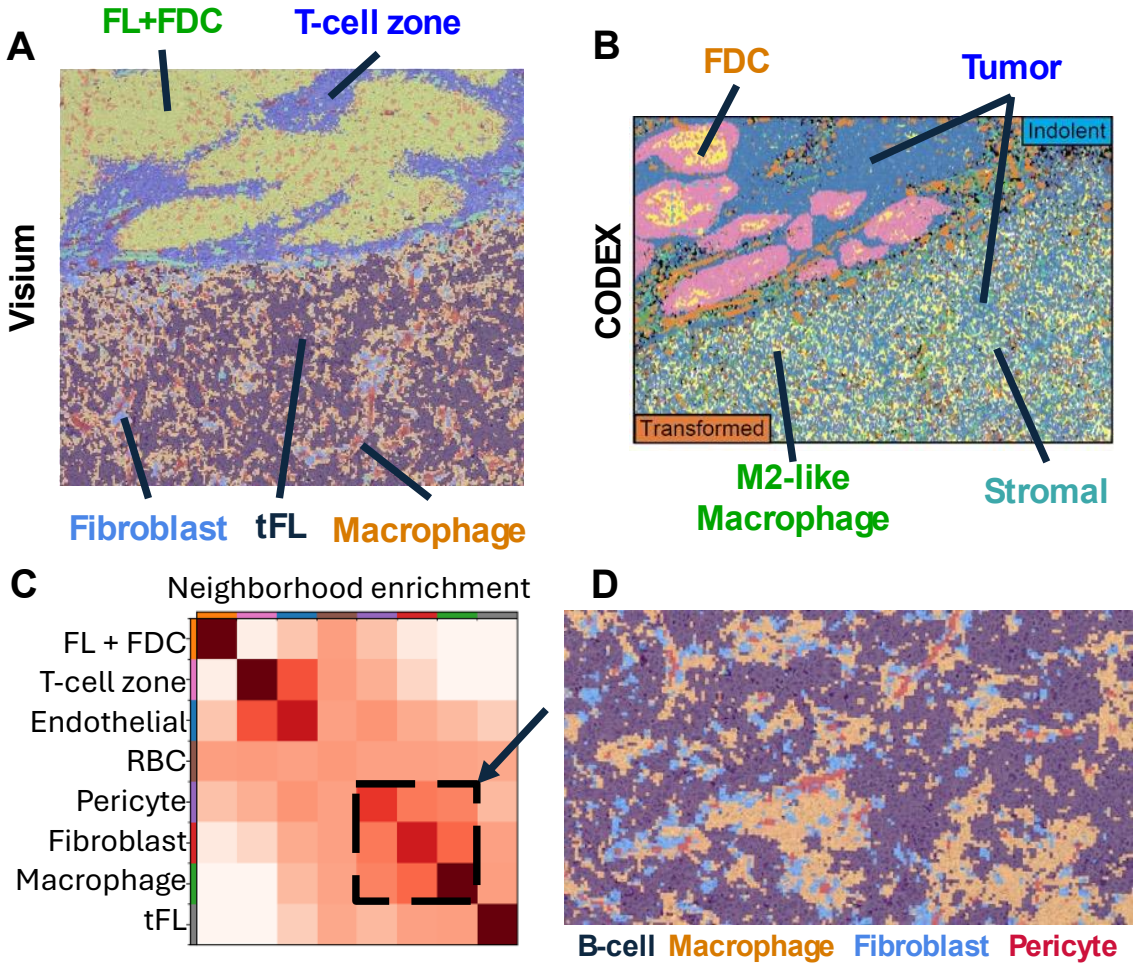

Figure 9. Visium HD in case FL-14 with admixed FL and tFL. A. Visium clustering across transformed FL regions (bottom of section) and indolent FL (top of section). FL: follicular lymphoma; FDC: follicular dendritic cells; tFL: transformed follicular lymphoma. **B**. Single-cell proteomic analysis by CODEX identifies cell types in adjacent tissue slice. **C**. Correlation matrix documents proximity of fibroblasts, pericytes, and macrophages. The normalized neighborhood enrichment score plotted in the figure quantifies the frequency that two cell types are neighbors normalized by the expected frequency if randomly distributed. **D.** Magnified section shows co-localized populations of macrophages, fibroblasts , and pericytes in tFL region.

References

1. Regev A, Teichmann SA, Lander ES, Amit I, Benoist C, Birney E, Bodenmiller B, Campbell P, Carninci P, Clatworthy M, Clevers H, Deplancke B, Dunham I, Eberwine J, Eils R, Enard W, Farmer A, Fugger L, Göttgens B, Hacohen N, Haniffa M, Hemberg M, Kim S, Klenerman P, Kriegstein A, Lein E, Linnarsson S, Lundberg E, Lundeberg J, Majumder P, Marioni JC, Merad M, Mhlanga M, Nawijn M, Netea M, Nolan G, Pe'er D, Phillipakis A, Ponting CP, Quake S, Reik W, Rozenblatt-Rosen O, Sanes J, Satija R, Schumacher TN, Shalek A, Shapiro E, Sharma P, Shin JW, Stegle O, Stratton M, Stubbington MJT, Theis FJ, Uhlen M, van Oudenaarden A, Wagner A, Watt F, Weissman J, Wold B, Xavier R, Yosef N, Human Cell Atlas Meeting Participants. The human cell atlas. Elife. 2017 Dec 5;6. PMCID: PMC5762154
2. Tian L, Chen F, Macosko EZ. The expanding vistas of spatial transcriptomics. Nat Biotechnol. 2023 Jun;41(6):773–782. PMCID: PMC10091579
3. Haradhvala NJ, Yiu S, Sadigh S, Beckmann L, Pospistle A, Deng S, Rivero S, Yeo Y, Maurer K, Shanmugam V, Van Orden M, Lu W, Li S, Livak KJ, Qiu H, Chang Y, Basak A, Shalek AK, McDonough MM, Redd RA, Rodig SJ, Gohil S, Neuberg DS, Wu CJ, Getz G, Jiang S, Parry EM. ASH 2024 Abstract 645: Cytokine-Linked Remodeling of the Immune Microenvironment Is a Hallmark of Transformation in Follicular Lymphoma [Internet]. [cited 2024 Dec 14]. Available from: https://ash.confex.com/ash/2024/webprogram/Paper200167.html
4. Alaggio R, Amador C, Anagnostopoulos I, Attygalle AD, Araujo IB de O, Berti E, Bhagat G, Borges AM, Boyer D, Calaminici M, Chadburn A, Chan JKC, Cheuk W, Chng W-J, Choi JK, Chuang S-S, Coupland SE, Czader M, Dave SS, de Jong D, Du M-Q, Elenitoba-Johnson KS, Ferry J, Geyer J, Gratzinger D, Guitart J, Gujral S, Harris M, Harrison CJ, Hartmann S, Hochhaus A, Jansen PM, Karube K, Kempf W, Khoury J, Kimura H, Klapper W, Kovach AE, Kumar S, Lazar AJ, Lazzi S, Leoncini L, Leung N, Leventaki V, Li X-Q, Lim MS, Liu W-P, Louissaint A, Marcogliese A, Medeiros LJ, Michal M, Miranda RN, Mitteldorf C, Montes-Moreno S, Morice W, Nardi V, Naresh KN, Natkunam Y, Ng S-B, Oschlies I, Ott G, Parrens M, Pulitzer M, Rajkumar SV, Rawstron AC, Rech K, Rosenwald A, Said J, Sarkozy C, Sayed S, Saygin C, Schuh A, Sewell W, Siebert R, Sohani AR, Tooze R, Traverse-Glehen A, Vega F, Vergier B, Wechalekar AD, Wood B, Xerri L, Xiao W. The 5th edition of the World Health Organization Classification of Haematolymphoid Tumours: Lymphoid Neoplasms. Leukemia. 2022 Jul;36(7):1720–1748. PMCID: PMC9214472
5. Campo E, Jaffe ES, Cook JR, Quintanilla-Martinez L, Swerdlow SH, Anderson KC, Brousset P, Cerroni L, de Leval L, Dirnhofer S, Dogan A, Feldman AL, Fend F, Friedberg JW, Gaulard P, Ghia P, Horwitz SM, King RL, Salles G, San-Miguel J, Seymour JF, Treon SP, Vose JM, Zucca E, Advani R, Ansell S, Au W-Y, Barrionuevo C, Bergsagel L, Chan WC, Cohen JI, d'Amore F, Davies A, Falini B, Ghobrial IM, Goodlad JR, Gribben JG, Hsi ED, Kahl BS, Kim W-S, Kumar S, LaCasce AS, Laurent C, Lenz G, Leonard JP, Link MP, Lopez-Guillermo A, Mateos MV, Macintyre E, Melnick AM, Morschhauser F, Nakamura S, Narbaitz M, Pavlovsky A, Pileri SA, Piris M, Pro B, Rajkumar V, Rosen ST, Sander B, Sehn L, Shipp MA, Smith SM, Staudt LM, Thieblemont C, Tousseyn T, Wilson WH, Yoshino T, Zinzani P-L, Dreyling M, Scott DW, Winter JN, Zelenetz AD. The International Consensus Classification of Mature Lymphoid Neoplasms: a report from the Clinical Advisory Committee. Blood. 2022 Sep 15;140(11):1229–1253. PMCID: PMC9479027
6. Radtke AJ, Roschewski M. The follicular lymphoma tumor microenvironment at single-cell and spatial resolution. Blood. 2024 Mar 21;143(12):1069–1079. PMCID: PMC11103101
7. Radtke AJ, Postovalova E, Varlamova A, Bagaev A, Sorokina M, Kudryashova O, Meerson M, Polyakova M, Galkin I, Svekolkin V, Isaev S, Wiebe D, Sharun A, Sarachakov A, Perelman G, Lozinsky Y, Yaniv Z, Lowekamp BC, Speranza E, Yao L, Pittaluga S, Shaffer AL, Jonigk D, Phelan JD, Davies-Hill T, Huang DW, Ovcharov P, Nomie K, Nuzhdina E, Kotlov N, Ataullakhanov R, Fowler N, Kelly M, Muppidi J, Davis JL, Hernandez JM, Wilson WH, Jaffe ES, Staudt LM, Roschewski M, Germain RN. Multi-omic profiling of follicular lymphoma reveals changes in tissue architecture and enhanced stromal remodeling in high-risk patients. Cancer Cell. 2024 Mar 11;42(3):444–463.e10. PMCID: PMC10966827
8. Han G, Deng Q, Marques-Piubelli ML, Dai E, Dang M, Ma MCJ, Li X, Yang H, Henderson J, Kudryashova O, Meerson M, Isaev S, Kotlov N, Nomie KJ, Bagaev A, Parra ER, Solis Soto LM, Parmar S, Hagemeister FB, Ahmed S, Iyer SP, Samaniego F, Steiner R, Fayad L, Lee H, Fowler NH, Flowers CR, Strati P, Westin JR, Neelapu SS, Nastoupil LJ, Vega F, Wang L, Green MR.

Follicular Lymphoma Microenvironment Characteristics Associated with Tumor Cell Mutations and MHC Class II Expression. Blood Cancer Discov. 2022 Sep 6;3(5):428–443. PMCID: PMC9894575
9. Traag VA, Waltman L, van Eck NJ. From Louvain to Leiden: guaranteeing well-connected communities. Sci Rep. 2019 Mar 26;9(1):5233. PMCID: PMC6435756
10. Goltsev Y, Samusik N, Kennedy-Darling J, Bhate S, Hale M, Vazquez G, Black S, Nolan GP. Deep Profiling of Mouse Splenic Architecture with CODEX Multiplexed Imaging. Cell. 2018 Aug 9;174(4):968–981.e15. PMCID: PMC6086938